INTERNATIONAL JOURNAL OF AUTOMOTIVE AND MECHANICAL ENGINEERING (IJAME)
ISSN: 2229-8649 e-ISSN: 2180-1606
VOL. 17, ISSUE 2, 7996 – 8010
DOI: https://doi.org/10.15282/ijame.17.2.2020.18.0599

ORIGINAL ARTICLE

Path Tracking Controller Design of Automatic Guided Vehicle Based on Four-Wheeled Omnidirectional Motion Model

Xiaojun Wu and Yang Yang

School of Mechanical and Electrical Engineering, Xi'an University of Architecture and Technology, Xi'an, China
Tel:+8613991229008

ABSTRACT – This paper presents a new design of omnidirectional automatic guided vehicle based on a hub motor, and proposes a joint controller for path tracking. The proposed controller includes two parts: a fuzzy controller and a multi-step predictive optimal controller. Firstly, based on various steering conditions, the kinematics model of the whole vehicle and the pose (position, angle) model in the global coordinate system are introduced. Secondly, based on the modeling, the joint controller is designed. Lateral deviation and course deviation are used as the input variables of the control system, and the threshold value is switched according to the value of the input variable to realise the correction of the large range of posture deviation. Finally, the joint controller is implemented by using the industrial PC and the self-developed control system based on the Freescale minimum system. Path tracking experiments were made under the straight and circular paths to test the ability of the joint controller for reducing the pose deviation. The experimental results show that the designed guided vehicle has excellent ability to path tracking, which meets the design goals.

ARTICLE HISTORY
Revised: 21st April 2020
Accepted: 29th June 2020

KEYWORDS
Automatic guided vehicle;
fuzzy control;
four-wheel independent steering;
path tracking;
hub motor.

INTRODUCTION

Automatic guided vehicle refers to a transport vehicle equipped with electromagnetic or optical automatic guiding devices, which can travel along the specified guiding path and has the functions of safety protection and load transfer [1, 2]. According to the number of guide wheels, it can be divided into two wheels [3], three wheels [4] and four wheels (4WS). At present, most of the guide wheels are composed of Mecanum wheels or ball wheels [5, 6]. There are two types of 4WS: four-wheel active steering vehicles (4WAS-AGV) [7] and four-wheel independent steering vehicles (4WIS-AGV) [8, 9]. The main advantage of 4WS is to maintain a side slip angle of the miniature vehicle and better dynamic response characteristics, and the vehicle can move in any direction in its working environment. In relevant research fields, a large number of studies have been carried out on automatic guided vehicles, such as AGV laser [10], vision [11, 12], positioning [13], navigation [14] and controller design [15]. Among them, the design of the control strategy is an essential task. The control strategy of path rectification is to obtain the pose (position, angle) deviation of the AGV through navigation technology (marker navigation, laser navigation and magnetic navigation [16]), and adjust the pose of the AGV in real-time by the control algorithm, to ensure the whole vehicle travels along the predetermined trajectory.

At present, many scholars are studying on different control methods to improve the AGV rectification effect. In China, Ren [17] proposed a vision-guided AGV based on Fuzzy PID to rectify the deviation, which effectively suppresses overshoot and shortens the stabilisation time. Meng [18] uses the improved PSO algorithm to optimise PID controller parameters, greatly enhancing the control precision to improve the tracking effect of the vehicle further. Zhao [19] studies the dynamic model and motion constraints of AGV and applies it to the navigation control process, while the precision of the trajectory tracking is difficult to guarantee. There are also numerous studies on developing controllers abroad to ensure the effectiveness of path trackings, such as optimal control [20], nonlinear decoupling control with observers [21], unknown disturbance observers [22] and multi-mode control strategy selector [23].

However, there are still great limitations in the study of the model of omnidirectional guide vehicle and of the control strategy of rectifying the position error in different magnitude ranges. Besides, the guide wheels mostly use Mecanum wheels or ball wheels currently. AGV vibration, slip, poor motion stability, and low control accuracy due to wheel structure [24], which is a challenge for AGV to adapt complex industrial production environments or move around in tight spaces.

In order to solve the above problems, this paper proposes a controller combining fuzzy control and multi-step predictive optimal control and uses it in a newly designed omnidirectional automatic guided vehicle based on a hub motor. This vehicle has various steering modes such as straight, horizontal, two-wheel steering, four-wheel steering, and zero-radius steering. It can move flexibly and freely in a small space and can carry different types of handling robots to meet diverse needs in industrial production. Finally, it is verified by experiments that the omnidirectional guided vehicle has

*CORRESPONDING AUTHOR | Xiaojun Wu | ✉ wuxiaojun@xauat.edu.cn

an excellent motion effect and rectifying ability, which can meet the demands of actual working conditions and can provide a reference for the application of AGV in the industrial field.

MATHEMATICAL MODEL

The designed omnidirectional steering mechanism is driven by four hub motors, and controlled by four independent steering motor to realise multiple moving modes such as straight, two-wheel steering, and four-wheel steering. The guiding mechanism works under medium and low-speed conditions, and the driving wheels use rigid tires. In addition, the guiding device is directly fastened to the frame without a suspension structure or mechanical transmission mechanism. Therefore, it can be assumed that the kinematic model is established in ideal conditions, that is, the whole vehicle is rigid, the ground level is horizontal, there is no relative sliding between the driving wheel and the ground, and the side-drifting or pitching motion will not occur during the running of the whole vehicle. Based on the above assumptions, a kinematic model based on 4WID-4WIS (four-wheel independent drive and four-wheel independent steering) AGV can be obtained.

Kinematics Models

Kinematics model under two front-wheel steering conditions

The two front wheel steering is the most common mode in the omnidirectional AGV steering. That is, during the steering, only the two front wheels are steered, and the rear wheels are kept in a straight route running state. In this process, the instantaneous center of the turning radius is on the imaginary axis of the rear of the vehicle body [25], as shown in Figure 1(a). In order to ensure that the four wheels rotate around the instantaneous centre of the vehicle, the linear velocity and the rotation angle of the driving wheel are calculated according to the relationship among the radius, the track and the wheelbase under steering conditions

In the steering mode of two front wheels, the turning radius of the vehicle R is:

$$\mathrm{R} = \mathrm{L}/\tan\delta \tag{1}$$

where: L is the wheelbase of the omnidirectional AGV ; δ is the angle between the actual speed direction of the front of the vehicle and the direction of the vehicle body.

The turning radius of the left and right wheels can be derived:

$$R_l = \mathrm{L}/\tan\delta + \mathrm{B}/2 \tag{2}$$

$$R_r = \mathrm{L}/\tan\delta - \mathrm{B}/2 \tag{3}$$

where: B is the track between the left and right wheels. The steering angle of each wheel obtained from Eq. (1) to (3) are:

$$\delta_{lf} = \arctan\left(L/(\mathrm{L}/\tan\delta + \mathrm{B}/2)\right) \tag{4}$$

$$\delta_{lf} = \arctan\left(L/(\mathrm{L}/\tan\delta - \mathrm{B}/2)\right) \tag{5}$$

$$\delta_{lr} = \delta_{rf} = 0 \tag{6}$$

Similarly, the speed of each wheel in the front wheel steering mode can be derived:

$$V_{lf} = V * (\mathrm{L}/\tan\delta + \mathrm{B}/2)/\{(\mathrm{L}/\tan\delta) * \cos\left[\arctan\left(\mathrm{L}/\left(\mathrm{L}/\tan\delta + \mathrm{B}/2\right)\right)\right]\} \tag{7}$$

$$V_{rf} = V * (\mathrm{L}/\tan\delta - \mathrm{B}/2)/\{(\mathrm{L}/\tan\delta) * \cos\left[\arctan\left(\mathrm{L}/\left(\mathrm{L}/\tan\delta - \mathrm{B}/2\right)\right)\right]\} \tag{8}$$

$$V_{lr} = V * (\mathrm{L}/\tan\delta + \mathrm{B}/2) * tan\delta/\mathrm{L} \tag{9}$$

$$V_{rr} = V * (\mathrm{L}/\tan\delta - \mathrm{B}/2) * tan\delta/\mathrm{L} \tag{10}$$

where, δ_{lf} - left front wheel steering angle; δ_{rf} - right front wheel steering angle; δ_{lr} - left rear-wheel steering angle; δ_{rr} - right rear-wheel steering angle; V_{lf} - left front wheel speed; V_{rf} - right front wheel speed; V_{lr} - left rear wheel Speed; V_{rr} - right rear wheel speed; V - the speed at the intersection of the medial axis of the vehicle and the virtual axis of the two front wheels.

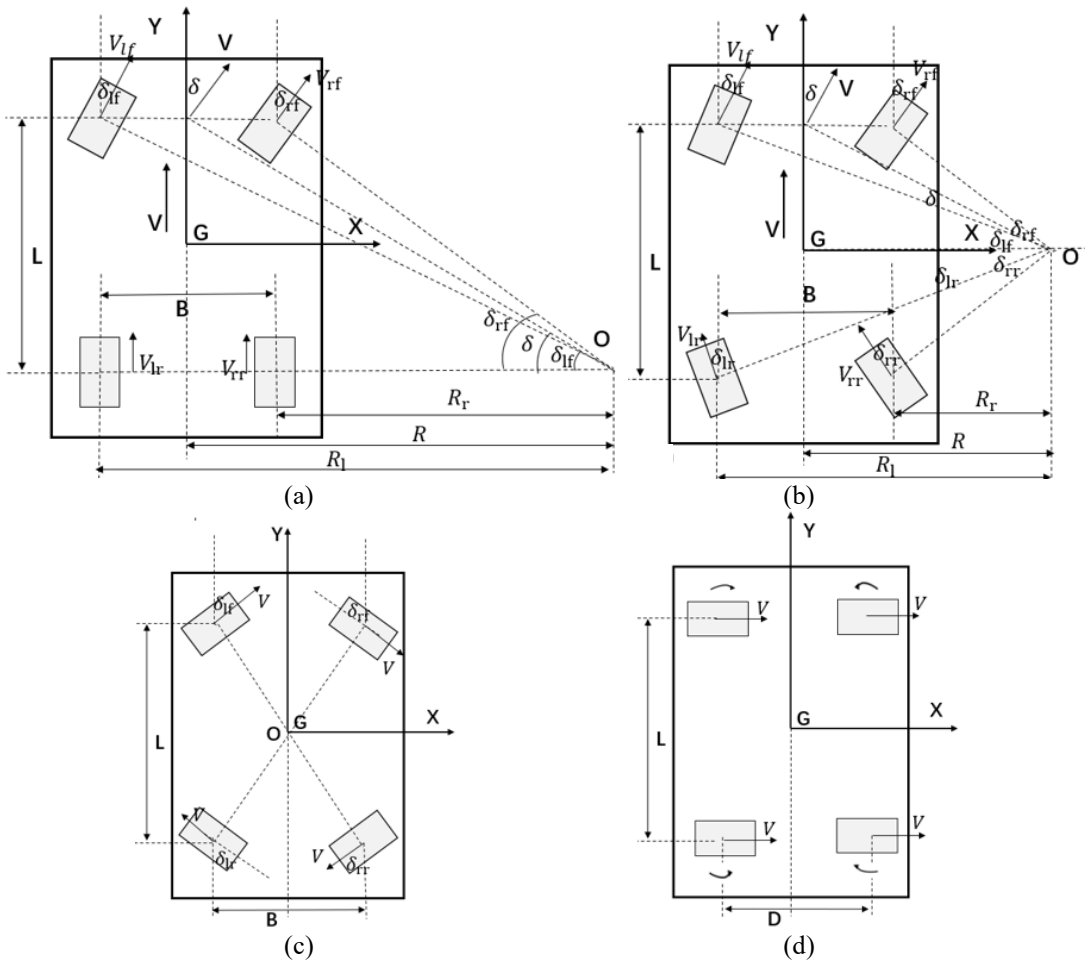

Figure 1. Steering model diagram under different working conditions

Kinematics model under four-wheel steering conditions

The four-wheel steering mode is a conventional steering mode, in which the four wheels are simultaneously steering during the steering of the vehicle, and the instantaneous centre of the motion is located on the extension line of the axle of the vehicle body (Figure 1(b)). In order to ensure that the four wheels are turned around the instantaneous centre of the vehicle, the relationship between the steering angle and speed of each wheel is calculated according to the characteristics of the four-wheel steering condition.

In the four-wheeled steering mode, the calculation method of the turning radius R of the vehicle and the turning radius of the left and right wheels can refer to Eq. (1) to (3).

$$\delta_{lr} = \delta_{lf} = \arctan\left(\mathrm{L}/\left(\mathrm{L}/\tan\delta + \mathrm{B}\right)\right) \tag{11}$$

$$\delta_{rr} = \delta_{rf} = \arctan\left(\mathrm{L}/\left(\mathrm{L}/\tan\delta - \mathrm{B}\right)\right) \tag{12}$$

The speed of each wheel is:

$$V_{lf} = V * \left(\mathrm{L}/2\tan\delta + \mathrm{B}/2\right)/\{(\mathrm{L}/2\tan\delta) * \cos\left[\arctan\left(\mathrm{L}/\left(\mathrm{L}/\tan\delta + \mathrm{B}\right)\right)\right]\} \tag{13}$$

$$V_{rf} = V * \left(\mathrm{L}/2\tan\delta - \mathrm{B}/2\right)/\{(\mathrm{L}/2\tan\delta) * \cos\left[\arctan\left(\mathrm{L}/\left(\mathrm{L}/\tan\delta - \mathrm{B}\right)\right)\right]\} \tag{14}$$

$$V_{lr} = V * \left(\mathrm{L}/2\tan\delta + \mathrm{B}/2\right) * 2tan\delta/\mathrm{L} \tag{15}$$

$$V_{rr} = V * \left(\mathrm{L}/2\tan\delta - \mathrm{B}/2\right) * tan\delta/\mathrm{L} \tag{16}$$

Kinematics model under zero-radius steering conditions

When the AGV operates in a relatively narrow space, an unconventional flexible steering mode, that is, a zero-radius steering mode is required. In this mode, each wheel is required to perform a significant rotation in the control state of 4WID-4WIS and is turned to the outside at the same time. When the extension line of the drive wheel during steering intersects at the geometric centre of the vehicle, the purpose of zero-radius steering achieved, as shown in Figure 1(c). At this time, the relationship between each steering angle of the whole vehicle and the driving wheel speed is as follows:

In this mode, the steering angle relationship between the left front wheel and the right rear wheel of the vehicle is:

$$\delta_{lf} = \delta_{rr} = \arctan(\mathrm{L/B}) \tag{17}$$

The steering angle relationship between the right front wheel and the left rear wheel is:

$$\delta_{rf} = \delta_{lr} = -\arctan(\mathrm{L/B}) \tag{18}$$

where the negative sign in the formula indicates that the steering angle of the wheel is in opposite directions.

The speed relationship of the four wheels is:

$$V_{lf} = V_{rf} = V_{lr} = V_{rr} \tag{19}$$

Kinematic model of lateral driving

When the whole vehicle is moving laterally, each wheel is turned outward at the same time until the steering angle of each wheel is reached at 90°, As shown in Figure 1(d). The relationship between the speed of each wheel in the horizontal driving mode is:

$$V_{lf} = V_{rf} = V_{lr} = V_{rr} \tag{20}$$

Pose Model of Omnidirectional AGV

Three DOF AGV developed in this paper can realise lateral movement, longitudinal movement, and rotational movement in planar space. As shown in Figure 2, ΣX'O'Y' is a global coordinate system fixed to the ground, and ΣXOY is a vehicle coordinate system that moves with the AGV body. Taking the two front wheel steering conditions as an example to analyse the pose model during the AGV movement, where M is the geometric centre of the AGV body, O_{lf} and O_{rf} are the wheel centres of the two front drive wheels, and N is the midpoint of the two front wheels. During the steering mode, the angle between the front wheel and the vehicle body is δ_{lf}, δ_{rf}; the wheel radius is r, the instantaneous turning radius:$\mathrm{O''M = R(t)}$; V_{lf}, V_{rf}, V are the instantaneous speeds of the left front wheel, the right front wheel, and the speed at the intersection of the medial axis of the vehicle and the virtual axis of the two front wheels respectively.

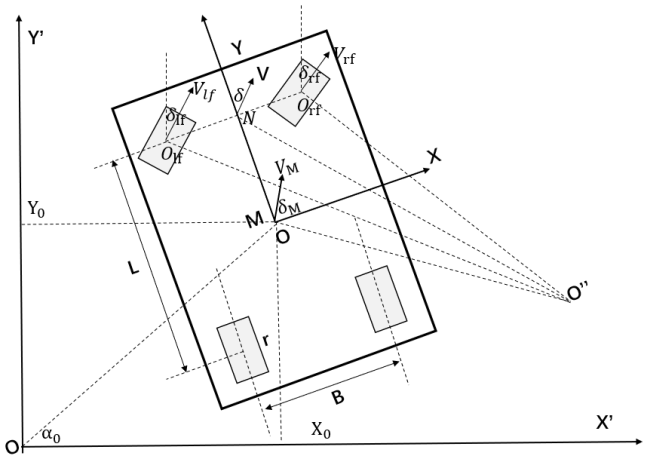

Figure 2. Pose model of omnidirectional AGV.

Let the omnidirectional parking position vector $\mathrm{P} = [\mathrm{X_0}, \mathrm{Y_0}, \alpha_0]^T$ at time t_0, After time Δt :

$$\omega_{lf}(\mathrm{t}) = \Delta\theta_{lf}/\Delta\mathrm{t} = \mathrm{d}\theta_{lf}/\mathrm{dt} \tag{21}$$

$$\omega_{rf}(\mathrm{t}) = \Delta\theta_{rf}/\Delta\mathrm{t} = \mathrm{d}\theta_{rf}/\mathrm{dt} \tag{22}$$

$$\mathrm{v}_{lf}(t) = r\omega_{lf}(t) \tag{23}$$

$$\mathrm{v}_{rf}(t) = r\omega_{rf}(t) \tag{24}$$

where: θ_{lf}, θ_{rf} respectively represents the rotation angle of the front drive wheel; ω_{lf}, ω_{rf} represent its corresponding angular velocity.

Analysis of Eq. (21) to (24) by the instantaneous method are:

$$\mathrm{V}(t) = \mathrm{V}_{lf}(t) * \frac{\sin(\delta_{lf} - \delta_{rf})}{sin\delta_{rf}} * \{1 + \left[\frac{\sin\delta_{rf}}{\sin(\delta_{lf} - \delta_{rf})}\right]^2 + \frac{\sin\delta_{rf} * \cos\delta_{lf}}{\sin(\delta_{lf} - \delta_{rf})}\}^{1/2} \tag{25}$$

From the principle of similar triangles;

$$\mathrm{V}_M(t) = V(t) * \cos\delta \tag{26}$$

From $\omega(t) = \mathrm{V}_M(t)/R(t)$;

$$\alpha(\mathrm{t}) = \alpha_0 + \int_{t_0}^{t} \omega(t)dt \tag{27}$$

where, $\alpha(\mathrm{t})$ is the angle between the vehicle centroid position and the ground coordinate system at time *t*.

From Eq. (21) to (25);

$$\mathrm{X(t)} = \mathrm{X_0} + cos\delta_M(t) \int_{t_0}^{t} v_M(t)dt \tag{28}$$

$$\mathrm{Y(t)} = \mathrm{Y_0} + sin\delta_M(t) \int_{t_0}^{t} v_M(t)dt \tag{29}$$

Then the pose vector of the omnidirectional vehicle at time *t* is:

$$\mathrm{P(t)} = [\mathrm{X(t)}, \mathrm{Y(t)}, \alpha(\mathrm{t})]^T \tag{30}$$

DEVIATION CORRECTED CONTROLLER DESIGN

The correction control system of this paper consists of a fuzzy controller, multi-step prediction optimal controller, and decoupling controller. The controller structure is illustrated in Figure 3. The lateral deviation, e_d, and the course deviation, e_θ, between the current pose and the ideal pose, calculated by the path tracking module, the image processing module and the AGV internal sensor; are transmitted to the vehicle controller through the CAN bus. The switching threshold of path tracking in the vehicle motion control program is ±6° and ±4 cm. When the deviation is higher than this value, the fuzzy controller was used. Otherwise, the program switches to the multi-step prediction optimal controller automatically. The output speed, U_d, and the output angle, U_θ, are decoupled by the decoupling controller and applied to the hub motor and the steering motor for correction. During the running of the vehicle, the servo control system continuously returns the real-time path deviation of the AGV, which is utilised to update the lateral deviation and course deviation in the correct control system.

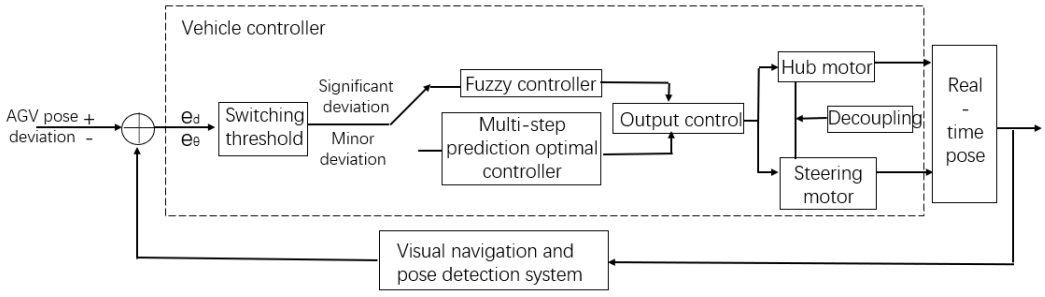

Figure 3. Control schematic of the joint control strategy.

Design of Multi-Step Prediction Optimal Controller

The AGV usually travels at time *t*, and after Δt time, it produces the course deviation Δe_θ and the lateral deviation Δe_d. According to the rigid translational principle, it can be known that:

$$\Delta \mathrm{e}_\theta/\Delta t = \omega = 2V_t tan\delta/L \tag{31}$$

$$\Delta \mathrm{e}_d/\Delta t = V_t cose_\theta \tag{32}$$

where: ω is the angular velocity of the vehicle body, $\omega = 2V_c tan\sigma$; V_t is the driving speed at time *t*.

According to the multi-step prediction iterative optimal control idea, the *N*-step iteration can reduce the course deviation and the lateral deviation to zero at the same time, namely:

$$e_\theta(N) = 0 \tag{33}$$

$$e_d(N) = 0 \tag{34}$$

When using multi-step iterative optimal control, the fastest correction can be achieved [26]:

$$J = 1/2 * \sum_{k=0}^{N-1} {\mu_k}^2 \tag{35}$$

where: k is the system control steps. In order to reduce the system controller's sensitivity to noise, enhance its anti-interference ability [27], and to consider an excessive lateral deviation will cause angular overshoot, and extreme steering angle of the front wheels will exceed the limits of the mechanical mechanism [28]. This paper sets the constraints as:

$$|e_d(k)| \le \Delta e_{dmax} \tag{36}$$

$$|e_\theta(k)| \le \Delta e_{\theta max} \tag{37}$$

$$|\Delta v| \le \Delta v_{max} \tag{38}$$

$$|\Delta a| \le \Delta a_{max} \tag{39}$$

where Δe_{dmax}, $\Delta e_{\theta max}$, Δv_{max}, and Δa_{max} are the maximum allowable lateral deviation, the maximum permissible course deviation, the maximum allowable drive wheel differential, and the maximum permissible drive wheel differential rate of change.

Assuming that the control period of the AGV is T, when the current pose state is k, the course deviation is e_θ and the lateral deviation is e_d. Establish the kinematic equation of lateral deviation and course deviation of the $k+1$ poses state, according to Eq. (31) and (32), under the constraint of the optimal deviation state equation:

$$e_\theta(k+1) = e_\theta(k) + 2V_k T_S tan\sigma / L \tag{40}$$

$$e_d(k+1) = e_d(k) - e_\theta(k) V_k T_S - V_k T_S tan\delta \tag{41}$$

Set the control quantity $\mu_k = tan\delta$, discretise the error deviation model and introduce it in the Lagrange pending number column to obtain the Hamilton optimal control function:

$$H_k = 1/2 * {\mu_k}^2 + {\lambda_{k+1}}^T * \left\{ \begin{bmatrix} e_\theta(k) \\ e_d(k) - e_\theta(k) V_k T_S \end{bmatrix} + \begin{bmatrix} \frac{2V_k T_S}{L} \\ -V_k T_S \end{bmatrix} \mu_k \right\} \tag{42}$$

The condition for obtaining the minimum value of the objective function formula (35) is:

$$\lambda_k = \partial H_k / \partial X_k \tag{43}$$

$$\partial H_k / \partial \mu_k = 0 \tag{44}$$

where, $X_k = [e_\theta(k), e_d(k)]^T$. Equation (43) and (44) can be derived as;

$$\mu_k = -(2V_k T_S / L) + \lambda_{2k} + (k+1) C V_k T_S \tag{45}$$

where: λ_{2k} and C are pending parameters. $e_\theta(k)$ and $e_d(k)$ can be derived by substituting Eq. (45) into Eq. (31) and (32) and then iteratively transforming. According to the target of the correction, that is, the value of the lateral deviation and the course deviation close to 0, the value of λ_{2k} and C can be obtained, and then substituted in Eq. (23), the control expression μ_k can be derived as;

$$\mu_k = -2Le_\theta(0) / V_k T_S N + \gamma [K - (N-1)/2] \tag{46}$$

where

$$\gamma = \{24Le_\theta(0) / (V_k T_S)^2 + [(24L / V_k T_S)^2 - (12LN / V_k T_S) - (12L / V_k T_S)] e_\theta(0)\} / (7N - N^3) \tag{47}$$

Under the constraint condition, the fastest and accurate correction can be obtained by the optimal control after N-step iteration.

Design of Fuzzy Controller

According to the analysis of the AGV motion model mentioned above, this AGV adopts the control mode of 4WID-4WIS, and the deviation of the overall path is the lateral deviation and the course deviation, which reflected on the control platform of the AGV. According to an analysis of the control characteristics of the guiding mechanism, a dual fuzzy controller, which consists of a fuzzy controller of speed and angle, can be established for path tracking. In this controller, the lateral deviation, e_d, and the course deviation, e_θ, of the running process are used as the input linguistic value, and output speed, U_d, and the output angle, U_θ, are used as output linguistic value. The fuzzy linguistic set is {NB (Negative Big), NM (Negative Medium), NS (Negative Small), O (Zero), PS (Positive Small), PM (Positive Medium), PB (Positive Big). The universe of discourse of the lateral deviation and the course deviation is [-1.2 m 1.2 m] and [-45 ° 45 °], respectively, and the quantisation level of the input linguistic value in the system is set to [-6, -5, -4, -3, -2, -1, 0, 1, 2, 3, 4, 5, 6].

A sharper, more sensitive membership function will be employed in the region with small path deviations. While in the larger path deviations region, a membership function with a gentle curve is utilised to enhance the stability and anti-interference ability of the controller. In the correct model, the weight of lateral deviation is greater than course, so lateral deviation requires a more sensitive membership function. According to the above design requirements, the distribution of membership functions of fuzzy input linguistic value e_d and e_θ is shown in Figure 4(a) and 4(c), and the distribution of membership functions of the fuzzy output linguistic value U_d and U_θ is shown in Figure 4(b) and 4(d).

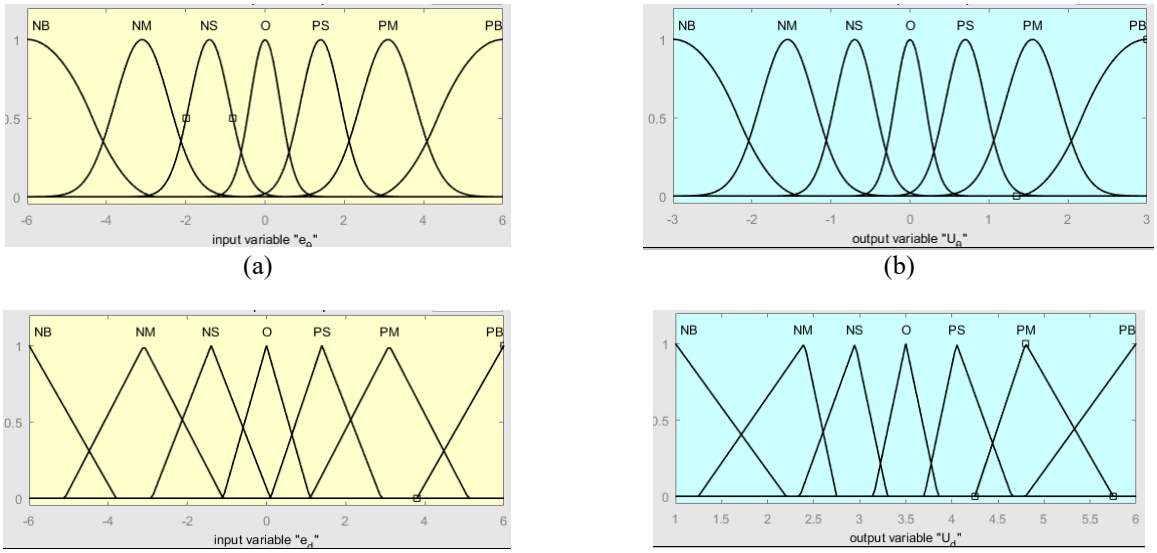

(a) (b) (c) (d)

Figure 4. Input-output variable membership function.

Design of Decoupling Controller

The omnidirectional AGV system designed in this paper can be regarded as a dual-input and dual-output system, and the control method based on the new multivariate reference model [29] is used for decoupling control. Set the actual output and the ideal output of the steering motor to be Y_1 and Y_{1m}, respectively, the actual output and the ideal output of the hub motor are Y_2 and Y_{2m}. G_{12} is the coupling effect of the steering motor on the hub motor. G_{21} is the coupling effect of the hub motor on the steering motor. G_{11} and G_{22} are the reference models of the two motors, respectively. R_n is the primary input of the *nth* channel. It can be derived from the decoupling principle of the reference model with dual-input and dual-output [29] as;

$$\mathrm{A} * \mathrm{B} = \mathrm{Y} \tag{48}$$

$$\mathrm{A} = \begin{bmatrix} G_{11} & G_{12} \\ G_{21} & G_{22} \end{bmatrix} \tag{49}$$

$$\mathrm{B} = (\mathrm{B}_1, \mathrm{B}_2) \tag{50}$$

$$\mathrm{B}_n = (\mathrm{R}_n - \mathrm{Y}_n)\mathrm{C}_n + (\mathrm{Y}_{nm} - \mathrm{Y}_n)\mathrm{C}_{nn} \tag{51}$$

$$\mathrm{Y} = (\mathrm{Y}_1, \mathrm{Y}_2) \tag{52}$$

where: $n=1, 2$.

Let $|\mathrm{A}| = \begin{bmatrix} G_{11} & G_{12} \\ G_{21} & G_{22} \end{bmatrix}$, where A_{in}-an algebraic complement of G_{in}, Y can be derived from the method of elimination:

$$Y_1 = \left[|A|(R_1C_1 + Y_{1m}C_{11}) - \sum_{n=1}^{2} Y_n A_{1n} \right] / [|A|(C_1 + C_{11}) + A_{11}] \tag{53}$$

Where:

$$Y_{1m} = R_1C_1G_{11}/(1 + C_1G_{11}) \tag{54}$$

$$R_1 = Y_{1m}(1 + C_1G_{11})/C_1G_{11} \tag{55}$$

C_{11} is the decoupling controller designed, and C_1 is the primary controller parameter.

Substituting Eq. (54) and (55) into Eq. (53) yields:

$$Y_{1m} + Y_{1m}\left\{ \frac{[|A| - G_{11}A_{11} - G_{11}(\sum_{n=1}^{2} Y_n A_{1n} - A_{11}Y_1)]}{[|A|G_{11}(C_1 + C_{11}) + G_{11}A_{11}]} \right\} = Y_1 \tag{56}$$

Y_2 can be calculated by the same reason. In the actual control system, the case $A=0$ is not considered. When $|A|\neq 0$, it can be concluded from the Eq. (31) that as long as the values of the second and third terms close to zero, the actual output approach that of ideal output. Reasonable design of the controller can achieve decoupling control of the system so that the steering motor and hub motor have a good input and output response.

ESTABLISHMENT OF THE EXPERIMENTAL DEVICE

The 4WID-4WIS AGV system developed in this paper is given in Figure 5. It comprises of a body platform, a four-wheeled driving system, a four-wheeled steering system and a vehicle vision system using a CCD industrial camera. The CAN was used for vehicle communication. The centre wheelbase of the 4WID-4WIS AGV is 1420 mm, the wheelbase of the left and right wheels is 1026 mm, the weight of the body equipped with the robot arm is 2470 kg, the maximum driving speed is 20 km/h, and the maximum acceleration is 0.5 m/s^2.

The guiding mechanism configuration of the system is shown in Figure 6, which includes steering and driving parts. When steering mode, the steering pinion rotates around the steering gear fixed on the frame to achieve a steering angle of ± 90 ° while eliminating the traditional steering rod mechanism and improving steering stability. The guiding tool adopts electromagnetic braking to integrate the brake pads on the braking shaft of the hub motor, which improves the positioning accuracy of the omnidirectional AGV. The steering and drive motors consist of four 5 kW servo motors and hub motors, respectively. All motors are accompanied by the encoder to obtain wheel angular velocity and steering angle.

(a) (b)

Figure 5. 4WID-4WIS system.

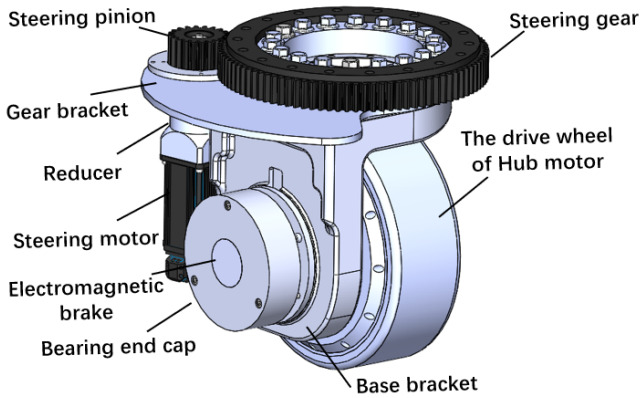

Figure 6. 4WID-4WIS guiding mechanism.

EXPERIMENT AND RESULT ANALYSIS

Four-Wheel Corner and Speed Output Experiment

In the 4WID-4WIS mode, the industrial PC is attached to the motion controller. Different vehicle body angles and speed were input on the self-developed upper computer to obtain the actual angle and speed of each wheel by the feedback of the angle and speed sensors (Figure7), experimental results take the average of multiple experiments. Among them, under the input of diverse body angles, the experimental data of the actual rotation angle of each wheel is shown in Figure 8(a). Different vehicle speed was input into the upper computer under the condition of the rated angle of 10°; the experimental data of each wheel output speed are given in Figure 8(b).

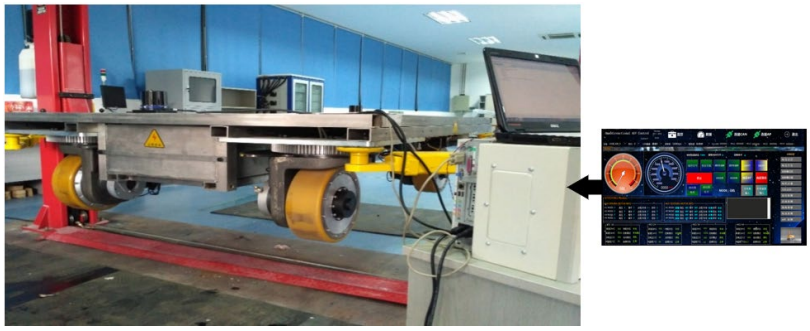

Figure 7. Experimental process of omnidirectional AGV steering angle and speed output.

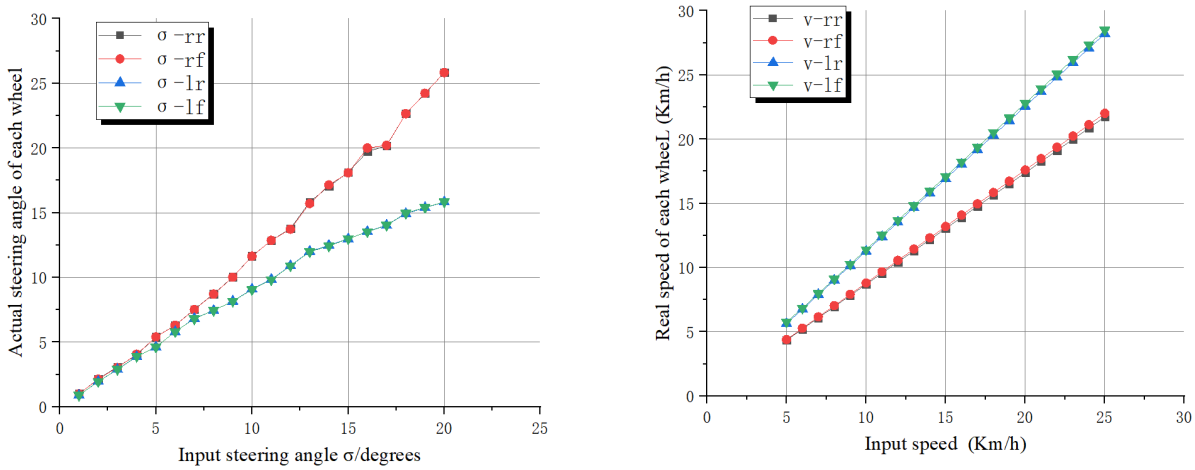

Figure 8. (a) Steering angle and (b) speed output experiment of four-wheels.

Through the four-wheel angle experiment and speed tests of the omnidirectional AGV, it can be concluded that:

i. When manually inputting different body angles, the actual output angle of the four wheels is about equal to the body input angle if the input value is small. When the input angle is large, there will be a particular regular shift of the actual output angle curve compared with the input, that is, the wheel angle on the right side is slightly larger than the left side. However, the average deviation of the output angle is kept within 0.8 °.

ii. In the case of rated angle, when the manual input speed is performed, the actual output speed of the left wheel is significantly higher than the right side, but the average deviation is controlled within 15 mm/s.

The reason why the actual output angle and speed of the left and right wheels were present on both sides of the vehicle input angle curve is that the turning of the vehicle in actual driving can be realised by the difference steering angle and speed of the left and right sides. The theoretical derivation of this part has been reflected in Eqs.1-20 above. In the angle and speed experiments, the average deviation of these two variables is controlled to a very small range, which indicates that the omnidirectional AGV has a decent steering angle and speed output response in the 4WID-4WIS control mode.

Path Tracking Correction Experiment

Straight path tracking experiments were performed on omnidirectional AGV. The experimental parameters are presented in Table 1. Figure 9 is the trial process of the correction on a straight path segment. The experimental tracking results are shown in Figure 10. During the control period, the correction process and the positional deviation in the straight path were recorded. The results obtained are shown in Figure 11:

Table 1. Experimental parameters of straight path tracking.

Parameters	Input speed (m/s)	Input angle (°)	Initial pose	Initial course deviation (°)	Initial lateral deviation (mm)
Value	0.5	0	(0,0)	30	500

Figure 9. Straight-line tracking experiment process of omnidirectional AGV.

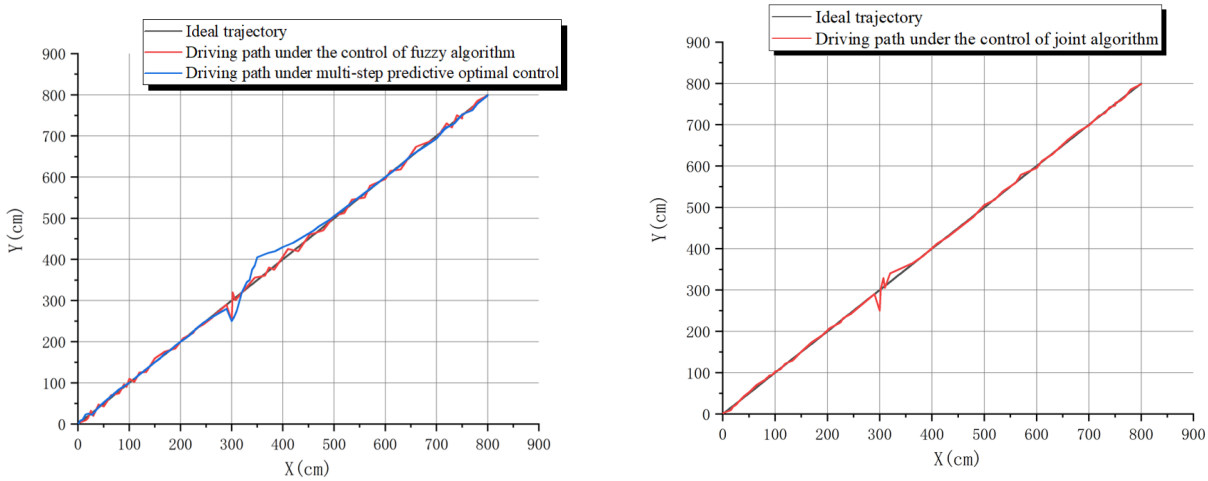

(a) (b)

Figure 10. Real-time trajectory when travelling straight-path tracking experiment (a) under separate control algorithm and (b) under joint control algorithm.

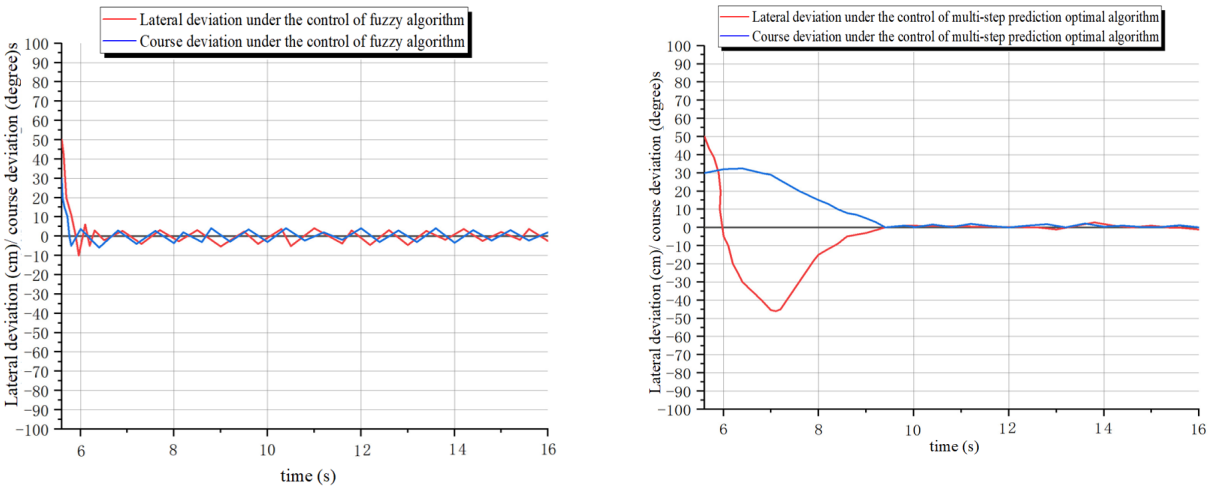

(a) (b)

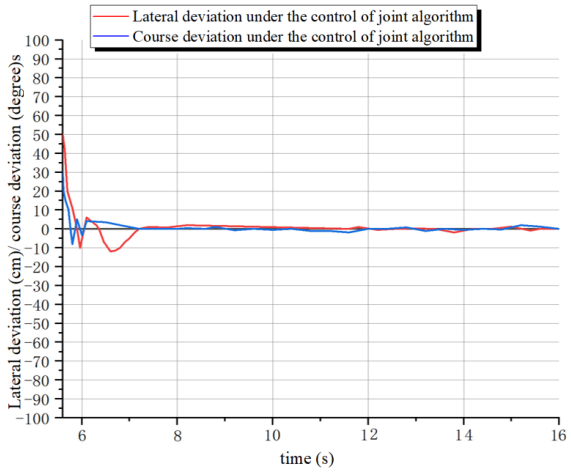

(c)

Figure 11. Correction process of course deviation and lateral deviation under straight-line tracking experiment by (a) fuzzy controller, (b) multi-step optimal controller and (c) joint controller.

Experimental data for tracking experiments of the circular path are presented in Table 2. The trial process and the real-time trajectory of the circular path are shown in Figure 12 and Figure13, respectively. The steering angle of the pose and lateral deviation were recorded during the control period. The corrective process of the vehicle is given in Figure 14.

Table 2. Experimental parameters of circular path tracking.

Parameters	Input speed (m/s)	Input angle (°)	The radius of the circular path (m)	Initial course deviation (°)	Initial lateral deviation (mm)
Value	0.5	0	4	20	400

Figure 12. Circular-line tracking experiment process of omnidirectional AGV.

Through the path tracking experiment of the omnidirectional AGV straight and circular path, the following conclusions can be concluded. If the fuzzy controller designed in this paper is used alone for path tracking and correction when the AGV has deviated, It is possible to make quick adjustments for significant pose deviation in a short time. However, there will always be oscillated during the correction process that follows, so that the overall path deviation cannot reach the steady state of the zero position. As shown in Figure 10(a) and Figure 11(a), in the straight path, 80 % of the initial 500 mm lateral deviation and 20 ° course deviation has been corrected by the fuzzy controller within 6s. However, due to the oscillation phenomenon, there is still more than 10 % deviation after the next 10 seconds. In the circular path tracking experiment, as showing in Figures 13(a) and 14(a). Only the speed of the correction is slightly higher than that of the straight path. However, the existence of the oscillation phenomenon makes the correction result still unsatisfactory. Therefore, the fuzzy control system alone has poor stability and low control accuracy.

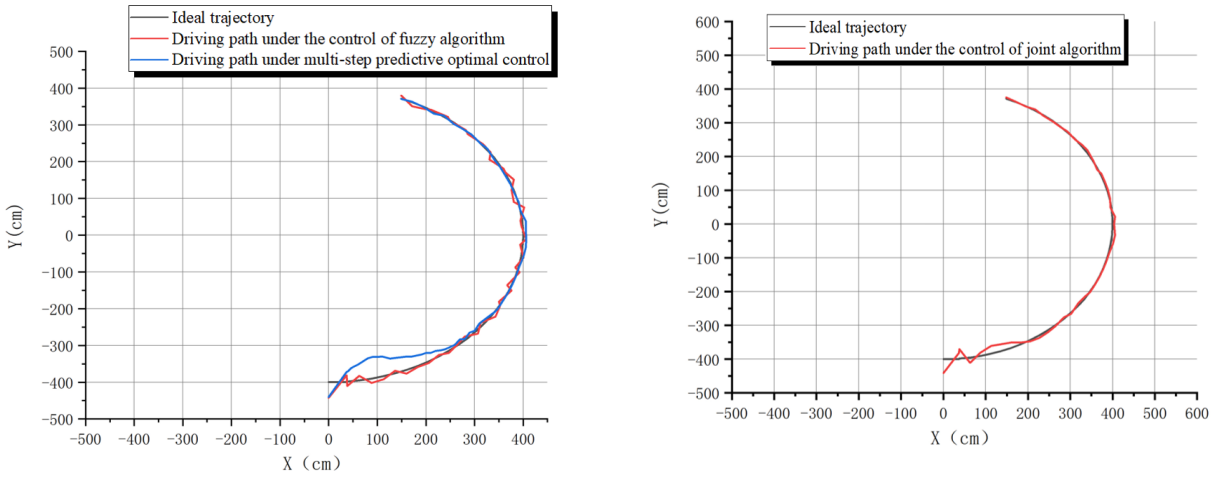

Figure 13. Real-time trajectory when travelling circular-path tracking experiment (a) under separate control algorithm and (b) under joint control algorithm.

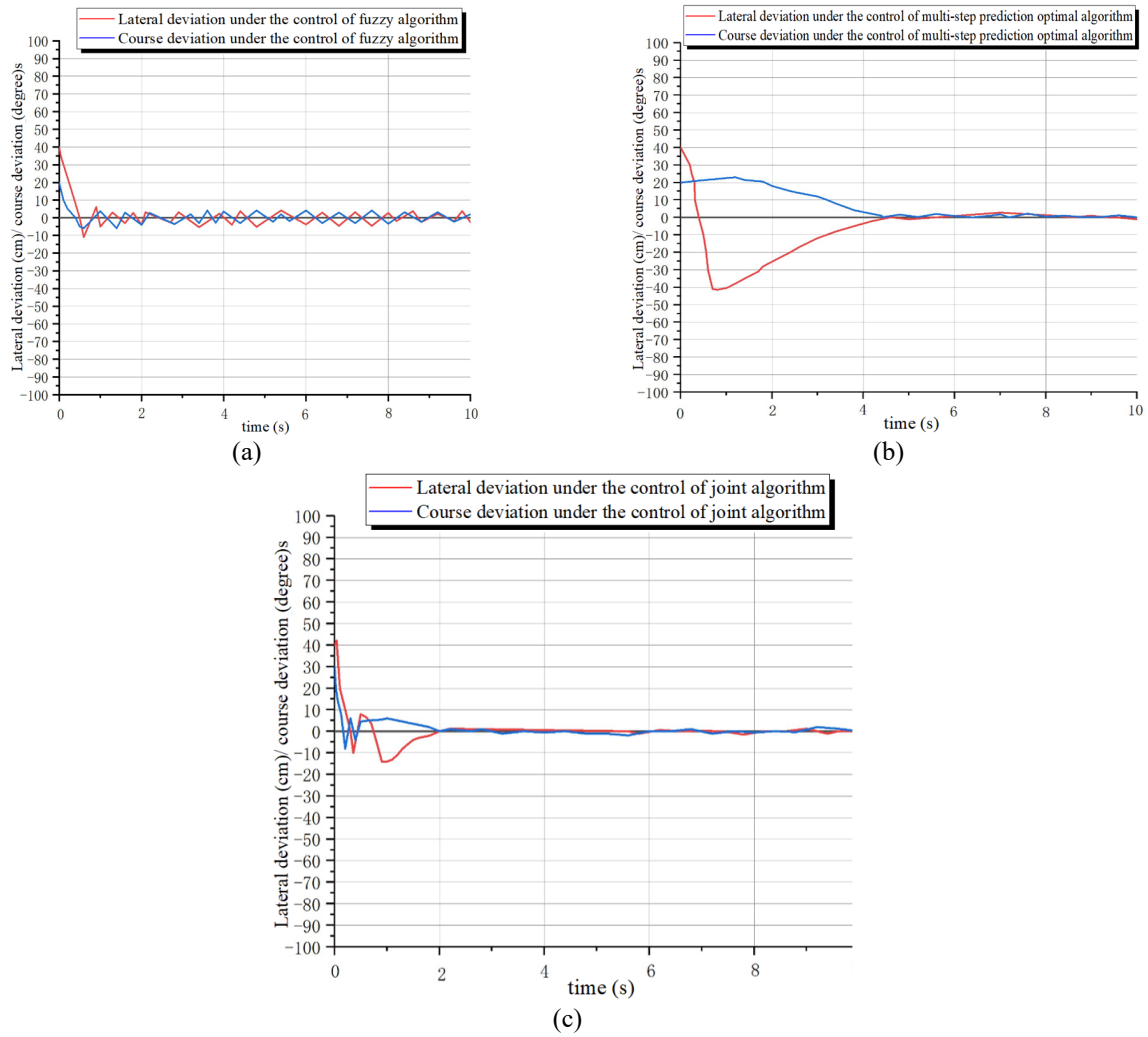

Figure 14. Correction process of course deviation and lateral deviation under circular-line tracking experiment. (a) Correction by Fuzzy controller. (b) By Multi-step optimal controller. (c) By the joint controller.

However, when the multi-step prediction optimal controller was used alone in the correction of the straight path which has large pose deviation, it is found that there is larger reverse adjustment quantity in the process of correction, and the iterative process of the algorithm is very complicated for the large pose deviation. Therefore, the use of multi-step prediction optimal controller alone in the correction process with large pose deviation will greatly affect the correction efficiency. When the multi-step prediction optimal controller was used solely in the straight path correction process, the controller started to produce a sizeable reverse adjustment quantity after 6 seconds, as shown in Figures 10(a) and 11(b). For a circular path in Figures 13(a) and 14(b), though the final correction curve is converged, the amount of reverse

adjustment quantity is also large. The existence of this phenomenon will have a greater impact on the control accuracy of the vehicle. According to the derivation process of the multi-step prediction optimal algorithm described above, it can be concluded that during the travelling along the circular path, the continuity steering makes the curvature radius have a particular impact on the pose deviation of the whole vehicle and the convergence tendency of the algorithm. However, it has no effect on its correcting effect. Lateral deviation and course deviation can be adjusted to reach zero at the same time, as shown in Figure 14(b), (c).

When the joint control algorithm using fuzzy control and multi-step predictive optimal control is used for correcting the deviation, according to the experimental results in Figure 11(c) and 14(c), when the pose deviation is relatively large, the use of fuzzy controller can reduce the pose deviation quickly. When the pose deviation is adjusted to a relatively small value, the program will automatically switch to the multi-step prediction optimal control algorithm to correct the path. At this time, more minor deviations lead to a smaller reverse adjustment quantity in the corrective process, which can significantly improve the correction efficiency and control precision.

Through the statistics of multiple experimental data of path tracking, it can be concluded that for the straight path tracking with an initial deviation of e_d=500 mm and e_θ=30°, the course deviation of the angle after the correction is controlled within 2°, the lateral deviation Within 6mm and the stable time is 7.2 s. For the initial deviation of e_d=400 mm and e_θ=20° in the circular path tracking, the average deviation of the angle after correction is controlled within 2 °, the distance deviation is controlled within 5.5 mm, and the stable time is 4 s. The experimental results for two-path tracking indicate that the omnidirectional AGV has excellent path tracking motion capability and meets the design requirements.

Table 3 lists the path tracking accuracy and the time to reach stability for different control methods. It can be seen from Table 3 that the path tracking algorithm proposed in this paper has a higher correction speed and has an excellent corrective ability for significant deviations.

Table 3. Accuracy and efficiency of different control methods.

Control method	Path tracking accuracy	Stable time/s	Initial deviation/mm
PID control[18]	$\|e_d\| \le 5.5$ mm	6.9~7.8	
Standard PSO control [18]	$\|e_d\| \le 3$ mm	4.0~6.2	
Integral separation PID [18]	$\|e_d\| \le 6$ mm		
Improved PSO control [18]	$\|e_d\| \le 2$ mm	2.7~4.3	
Control based on pose state and limited control steps [26]	$\|e_d\| \le 2$ mm, $\|e_\theta\| \le 2$ °	0.8~1.2	
Variable structure control [30]		4~5	
State feedback control [16]	$\|e_d\| \le 130$ mm		
Control based on optimal deviation path [31]	$\|e_d\| \le 6$ mm		50.8 mm
Controller based on backstepping method [32]	$\|e_d\| \le 20$ mm, $\|e_\theta\| \le 1$ °		For circular-line tracks with a radius of 1m
Fuzzy control used alone in this paper	For straight-line : $\|e_d\| \le 40$ mm, $\|e_\theta\| \le 3$ °	Oscillation	e_d=500 mm, e_θ=30 °
	For circular-line : $\|e_d\| \le 35$ mm, $\|e_\theta\| \le 4$ °	Oscillation	e_d=400 mm, e_θ=20 °
Multi-step optimal control used alone in this paper	For straight-line : $\|e_d\| \le 10$ mm, $\|e_\theta\| \le 2$ °	9.3	e_d=500 mm, e_θ=30 °
	For circular-line : $\|e_d\| \le 9$ mm, $\|e_\theta\| \le 2$ °	4.2	e_d=400 mm, e_θ=20 °
The joint controller used alone in this paper	For straight-line : $\|e_d\| \le 6$ mm, $\|e_\theta\| \le 2$ °	7.2	e_d=500 mm, e_θ=30 °
	For circular-line : $\|e_d\| \le 5.5$ mm, $\|e_\theta\| \le 2$ °	4	e_d=400 mm, e_θ=20 °

CONCLUSION

This paper presented an automatic guided vehicle based on a hub motor and proposed a joint controller for the guided vehicle to track the established trajectories. The kinematic model of the car is introduced based on numerous steering conditions, and the pose model in the global coordinate system is established. Based on the modelling, the controller is designed based on fuzzy control and multi-step prediction optimal method. The pose deviation is used as the input variable of the control system, and the threshold is switched according to the value of the input variable. By switching between different control methods to correction significant pose deviation. The steering angle and speed output experiments were conducted to verify the ability of output response of the whole AGV, and another set of experiments was done to verify the rationality and the effectiveness of the designed controller by controlling the omnidirectional AGV to track the straight and circular path:

i. In the steering angle and the speed output experiment, the average deviation of the four-wheel output steering angle is within 0.8°, and the average deviation of the rotation speed is 15 mm/s;

ii. Within the path tracking test, the results of multiple experimental results show that for the initial deviation of e_d=500 mm and e_θ=30° in the straight path tracking, the average deviation of the angle after the correction is controlled within 2 °, the distance deviation is controlled within 6 mm, and the controller system stabilises after 7.2 seconds. For the initial deviation of e_d=400 mm and e_θ=20° in the circular path tracking, the average deviation of the angle after the correction is controlled within 2°, the distance deviation is controlled within 5.5 mm, and the stable time is 4 s.

Experiments show that the omnidirectional AGV has good path tracking performance under the control mode of 4WID-4WIS, which meets the design requirements.

ACKNOWLEDGEMENT

This research was supported by the National Natural Science Foundation of China (51475353), and by Xi'an Science and Technology Project (2020KJRC0049).

REFERENCES

[1] Chenchen S, Peihuang L, Xing W. Collaborative calibration of initiative multi-camera guiding system for transport automatic guided vehicle. Chinese Journal of Scientific Instrument, 2014; 35(11): 2589-2599.

[2] Bin W, Xiaoming Q, Xing W. Optimization design on AGV frame structure. China Mechanical Engineering, 2014; 25(19): 2653-2657.

[3] Kewei H. Research on navigation and obstacle avoidance technology of automatic guided vehicle AGV. Zhejiang: Zhejiang University; 2012.

[4] Han Z, Xiaohong Y, Yanming W. Nonlinear model predictive control of trajectory tracking for nonholonomic AGV. China Mechanical Engineering, 2011; 22(6): 681-686.

[5] Shuguang W. Principles and design of mobile robots. Beijing: People's Posts and Telecommunications Press; 2013.

[6] Wei T, Yong L, Haixiu H et al. Kinematics analysis and self-adaptive controller design of omni-directional movement platform. Mechanical Science and Technology for Aerospace Engineering, 2017; 36(6): 883-889.

[7] Li B, Fan Y. Optimal model following control of four-wheel active steering vehicle. In: International Conference on Information & Automation, pp. 1-3; 2009.

[8] Selekwa MF, Nistler JR. Path tracking control of four wheel independently steered ground robotic vehicles. In: 2011 50th IEEE Conference on Decision And Control And European Control Conference, Orlando, FL; 12-15 October, 2011.

[9] Wada M.. Virtual link model for redundantly actuated holonomic omnidirectional mobile robots. In: 2006 IEEE International Conference on Robotics And Automation, Orlando, FL; 15-19 May, 2006.

[10] Bui T L , Doan P T , Kim H K , et al. Trajectory tracking controller design for AGV using laser sensor based positioning system. In: Asian Control Conference; 23 September, 2013.

[11] Kang J, Lee J, Eum H et al. An Application of Parameter Extraction for AGV Navigation Based on Computer Vision. In: 10th International Conference on Ubiquitous Robots And Ambient Intelligence, Jeju, South Korea; Oct 30-Nov 02, 2013.

[12] Kotze B , Jordaan G , Vermaak H . Reconfigurable navigation of an Automatic Guided Vehicle utilising omnivision. In: 2013 6th Robotics and Mechatronics Conference (RobMech); 19 December,

[13] Cho H , Song H , Park M , et al. Independence localization system for Mecanum wheel AGV. In: Ro-man; 26-29 August, 2013.

[14] Li Z M, Weng X, Su Z Y et al. A navigation method of information fusion and mutual aid based on map for logistic AGV. In: 6th International Conference on Measuring Technology and Mechatronics Automation (ICMTMA), Zhangjiajie, China; 10-11 January, 2014.

[15] Hung N, Im J S, Jeong S K et al. Design of a sliding mode controller for an automatic guided vehicle and its implementation. International Journal of Control Automation and Systems, 2010; 8(1): 81-90.

[16] Wuwei C, Haitao S, Bichun L et al. Tracking control of automatic guided vehicles based on navigation line navigation. Chinese Journal of Mechanical Engineering, 2006; 42(8): 164-170.

[17] Keyan R, Xingsheng G, Jingping H et al. Correction control of AGV based on fuzzy PID. Control Engineering of China, 2006; 1(2): 12.

[18] Wenjun M, Zhongqiang L. Research on the path tracking control for vision-guided AGV. Control Engineering of China, 2014; 21(3): 5.

[19] Lei Z, Hongpeng W, Liang D et al. A drift control method for high-speed wheeled mobile robot based on dynamic model. Robot, 2014; 36(2): 9.

[20] Amdouni I, Jeddi N, El Amraoui L et al. Optimal control approach developed to four-wheel active steering vehicles. In: 5th International Conference on Modeling, Simulation and Applied Optimization (ICMSAO), Hammamet, TUNISIA; 28-30 April, 2013.

[21] Chen C, Jia Y. Nonlinear decoupling control of four-wheel-steering vehicles with an observer. International Journal of Control Automation & Systems, 2012; 10(4): 697-702.

[22] HS K, SS Y. Estimation of vehicle sideslip angle for four-wheel steering passenger cars. Transactions on Control, Automation and Systems Engineering, 2001; 3(2): 71-76.

[23] Yang Z, Wang Z, Su W et al. Multi-mode control method based on fuzzy selector in the four wheel steering control system. In: IEEE International Conference on Control & Automation, 2010.

[24] Gosselin C, Angeles J. Singularity analysis of closed-loop kinematic chains. IEEE Transactions on Robotics And Automation, 1990; 6(3): 281-290.

[25] Xiaopei L. Research on the full steering system of space-saving electric vehicle based on hub motor. Chengdu: Southwest Jiao Tong University; 2015.
[26] Xiaoming Q, Liqun Z, Peihuang L et al. Optimal path tracking control method of omni-directional mobile AGV based on pose state. Transactions of the Chinese Society for Agricultural Machinery, 2018; 49(4): 6.
[27] Jun Y, Xiaoming Q, Peihuang L et al. Recognition and Accurate measurement of vision-guided path of automatic guided vehicle. Journal of South China University of Technology. Natural Science Edition, 2012; 40(3): 6.
[28] Rongben W, Bing L, Youchun X et al. Optimal controller design of intelligent vehicle autonomous navigation based on visual navigation. Automotive Engineering, 2001; 21(2): 4.
[29] Cheng L, Fuyu Z, Suxia H et al. A reference model decoupling method for multivariable systems. Control Engineering of China, 2009; 16(1): 4.
[30] Wanjun W, Weigong Z, Zongyang G. Path tracking control of automatic guided vehicle. Measurement & Control Technology, 2009; 28(9): 3.
[31] Zai L, Yingqi T, Dong L et al. AGV rectifying method based on optimal deviation path. Chinese Journal of Scientific Instrument, 2017; 38(4): 7.
[32] Setiawan YD, Nguyen TH, Pratama PS et al. Path tracking controller design of four wheel independent steering automatic guided vehicle. International Journal Of Control Automation And Systems, 2016; 14(6): 1550-1560.